PHYSICAL REVIEW B **85**, 214120 (2012)

Incipient ferroelectricity in 2.3% tensile-strained $CaMnO_3$ films

T. Günter,[1] E. Bousquet,[2,3] A. David,[4] Ph. Boullay,[4] Ph. Ghosez,[3] W. Prellier,[4] and M. Fiebig[1,2]
[1]*HISKP, Universität Bonn, Nussallee 14-16, 53115 Bonn, Germany*
[2]*Department of Materials, ETH Zurich, Wolfgang-Pauli-Strasse 10, 8093 Zurich, Switzerland*
[3]*Physique Théorique des Matériaux, Université de Liège, Allée du 6 août, 17, 4000 Sart Tilman, Belgium*
[4]*Laboratoire CRISMAT, CNRS UMR 6508, ENSICAEN, 6 Boulevard Maréchal Juin, 14050 Caen Cedex 4, France*
(Received 29 November 2011; revised manuscript received 20 April 2012; published 20 June 2012)

Epitaxial $CaMnO_3$ films grown with 2.3% tensile strain on (001)-oriented $LaAlO_3$ substrates are found to be incipiently ferroelectric below 25 K. Optical second harmonic generation (SHG) was used for the detection of the incipient polarization. The SHG analysis reveals that $CaMnO_3$ crystallites with in-plane orientation of the orthorhombic b axis contribute to an electric polarization oriented along the orthorhombic a (respectively c) axis in agreement with the predictions from density functional calculations.

DOI: 10.1103/PhysRevB.85.214120 PACS number(s): 77.55.Nv, 77.80.bn, 71.15.Mb, 42.65.Ky

I. INTRODUCTION: MULTIFERROICS WITH STRAIN-DRIVEN FERROELECTRICITY

Control of the magnetic response by electric fields and of the dielectric response by magnetic fields is highly interesting for spintronics applications and devices based on a rigid coupling of magnetic and dielectric properties. The possibly most fertile source for magnetoelectric cross correlations are compounds with a coexistence of magnetic and electric long-range order, called multiferroics.[1,2] The magnetoelectric phase coexistence is inherently rare: The established mechanisms driving magnetic and ferroelectric order require partially filled and empty $3d$ orbitals, respectively, and are therefore mutually exclusive unless they arise from different lattice sites.[3,4] This led to an intense search for alternative mechanisms promoting ferroelectricity in the presence of long-range magnetic order. A variety of mechanisms have been identified up to now.[5] One of the most notable examples is $BiFeO_3$, the only robust ambient multiferroic, in which ferroelectricity is driven by an electronic $6s$ lone pair of the Bi^{3+} ions. Furthermore, in compounds where the magnetic long-range order breaks the inversion symmetry and induces a spontaneous polarization the magnetoelectric effects are intrinsically strong because of the rigid coupling of the improper ferroelectric polarization to the proper magnetic order parameter(s).[2,6–9]

In spite of the impressive magnetoelectric coupling effects observed in some of these compounds an ambient multiferroic with pronounced and strongly coupled magnetization and polarization has not been discovered thus far. As a consequence, the ambition to discover fundamentally new mechanisms promoting multiferroic order is unbroken. In the past, new multiferroics were usually obtained via the chemical route by synthesizing materials from chemical building blocks with a high potential to promote multiferroic order. As an alternative it was recently suggested to take a structural route and modify the unit cell parameters of non-multiferroic compounds until they develop the magnetoelectric phase coexistence. An efficient way to achieve this is strain. The improvement in thin-film growth technologies in the past years allows the growth of thin films with epitaxial strains of several percent.[10] Such strain can be used for increasing ferroelectric[11] and ferromagnetic[12,13] transition temperatures, induce ferroelectricity,[14] or enhance the magnetization of a ferromagnet.[15] In 2010 it was shown that tensile biaxial strain of 1.1% pushes $EuTiO_3$ into a multiferroic state by inducing a spontaneous polarization estimated as 29 $\mu C/cm^2$ that coexists with a ferromagnetic phase.[16] First-principles density functional calculations explained this transition by a softening of a polar phonon mode driven by spin-phonon coupling.[17]

Aside from this landmark experiment, strain-induced ferroelectricity complementing magnetic order was also predicted for EuO and $CaMnO_3$. For EuO, epitaxial tensile or compressive strain in the order of as much as 4% is required,[18] which is difficult to achieve experimentally. $CaMnO_3$ is a particularly attractive candidate compound. First, the threshold tensile epitaxial strain required for stabilizing a ferroelectric phase was predicted to be a moderate 2.1%.[19] Second, multiferroic $CaMnO_3$ would create an interesting exception to the aforementioned $3d^0$ rule because, in contrast to other multiferroic perovskite oxides, antiferromagnetism and ferroelectricity in $CaMnO_3$ would both be associated to the Mn^{4+} cation site. At the bulk level, the antiferrodistortive structural instability is calculated to dominate the ferroelectric instability, so that the ground state is nonpolar. However, epitaxial tensile strain is expected to promote the polar mode to the extent that the compound can eventually become spontaneously polarized in thin films. Third, "chemical strain" exerted by replacing Ca by $Sr_{0.55}Ba_{0.45}$ in bulk crystals already revealed the emergence of a ferroelectric state.[20]

Unfortunately, the experimental verification of ferroelectricity in strained $CaMnO_3$ films remained an unsolved task thus far. For $CaMnO_3$ a polarization of 4 $\mu C/cm^2$ was predicted to emerge (at 0 K) along the orthorhombic a axis for tensile strain of 2.1% applied in the orthorhombic ac plane.[19] This value is at least an order of magnitude larger than the spontaneous polarization obtained in the magnetically induced ferroelectrics.[7,8] However, pyroelectric current measurements are spoiled by leakage currents and by the inefficiency of generating electric poling fields and pyrocurrents within the film plane. A more suitable experimental approach for the verification of in-plane ferroelectricity is clearly required.

Here we report the presence of an incipient ferroelectric state below 25 K in epitaxial $CaMnO_3$ films subjected to 2.3% tensile strain. Incipient ferroelectrics are compounds with emerging electric-dipolar long-range order where the

Curie-Weiss temperature $T_{\rm CW}$ is so close to zero (either $T_{\rm CW} \gtrsim 0$ or $T_{\rm CW} \lesssim 0$) that the long-range-ordered state is not yet stabilized down to 0 K.[21–25] Incipient ferroelectrics with $T_{\rm CW} \gtrsim 0$ are sometimes termed "quantum paraelectrics"[26–28] when the suppression of the ferroelectricity is related to quantum fluctuations and distinguished from the "incipient ferroelectrics" in a narrower sense. However, here we follow the majority of published work and refrain from making this distinction. One of the best known incipient ferroelectrics is $\rm SrTiO_3$ ($T_{\rm CW} > 0$)[26,29] so that we use it as reference compound to which we compare our $\rm CaMnO_3$ data.

The polarizability of the $\rm CaMnO_3$ films is demonstrated by optical SHG. The direction of the incipient polarization is derived from symmetry considerations and found to be oriented diagonally between the principal in-plane axes associated with the cubic perovskite subcell of the pseudocubically grown films. This orientation agrees with earlier predictions derived from density functional calculations; here a refined density functional approach backs up our conclusions.

II. PROBING FERROELECTRICITY BY SHG

SHG is a well-established tool for probing ferroic order in bulk crystals and thin films.[30,31] The nonlinear optical process describes the generation of a light wave at the frequency 2ω in a material with ω as the frequency of the incident light.[32] This is described by the expression $P_i(2\omega) = \varepsilon_0 \chi_{ijk} E_j(\omega) E_k(\omega)$. The component χ_{ijk} of the nonlinear susceptibility tensor couples j and k polarized contributions of the electric field $\vec{E}(\omega)$ of the incident light to an i polarized contribution to the polarization $\vec{P}(2\omega)$ driving the SHG light field. In the electric-dipole approximation $\hat{\chi}$ is a polar tensor so that components $\chi_{ijk} \neq 0$ are obtained in noncentrosymmetric systems only.[32] Thus, SHG is well suited for detecting ferroelectric order breaking the inversion symmetry.[33] In contrast to linear optical techniques the ferroelectric SHG signal emerges free of background at the Curie temperature. SHG is particularly useful for probing leaky or in-plane ferroelectricity because, in contrast to pyrocurrent measurements, the finite conduction does not interfere with the detection of the spontaneous polarization and electrodes are not applied. In addition, the degree of freedom of spatial resolution inherent to optical techniques allows one to probe the spatial distribution of the spontaneous polarization and, hence, image domains.

III. PEROVSKITE SUBCELLS IN PSEUDOCUBIC SAMPLES

Bulk $\rm CaMnO_3$ crystallizes in a distorted orthorhombic structure described by the space group *Pnma*.[34] In orthorhombic coordinates the lattice parameters are $a = 5.279$ Å, $b = 7.448$ Å, and $c = 5.264$ Å. This structure possesses a perovskite subcell that can be approximated with $a/\sqrt{2} \approx b/2 \approx c/\sqrt{2} \approx a_{\rm cube} = 3.72$ Å as cubic lattice parameter as shown in Fig. 1. Below $T_N = 122$ K $\rm CaMnO_3$ exhibits a G-type antiferromagnetic order. According to Ref. 19, a polar ground state is obtained for tensile strains larger than 2.1% for which a cubic substrate with $a_{\rm cube} \geqslant 3.80$ Å is required.

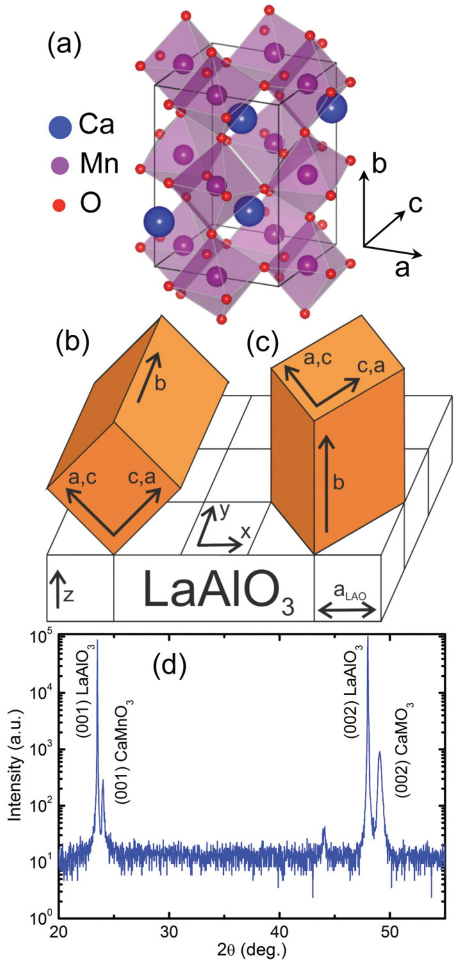

FIG. 1. (Color online) Orthorhombic unit cell of $\rm CaMnO_3$ and possible orientations of $\rm CaMnO_3$ grown on $\rm LaAlO_3$. (a) Orthorhombic unit cell of $\rm CaMnO_3$. (b),(c) Principal orientations of $\rm CaMnO_3$ grown on $\rm LaAlO_3$ with (b) in-plane and (c) out-of-plane orientation of the orthorhombic b axis. The orthorhombic axes are denoted as a, b, c, whereas the pseudocubic axes are denoted as x, y, z, with $a_{\rm LAO}$ as the pseudocubic unit cell parameter. (d) θ-2θ XRD scan of a typical strained $\rm CaMnO_3$ film epitaxially grown on $\rm LaAlO_3$. The peak at 44° is caused by the sample holder.

Our $\rm CaMnO_3$ films (thickness 40 nm) were grown on (001)-oriented $\rm LaAlO_3$ substrates with $a_{\rm LAO} = 3.81$ Å as lattice constant of the pseudocubic subcell. This corresponds to 2.3% tensile strain of the films. Pulsed laser deposition was used for the epitaxial growth of the $\rm CaMnO_3$ films. The substrates were kept at a constant temperature of 650 °C during the deposition, which was carried out at a pressure of 0.04 mbar of flowing oxygen. After the deposition, the samples were cooled to 400 °C maintaining the same conditions. The oxygen pressure was then increased to 300 mbar, followed by slow cooling to room temperature. The structural study was carried out by x-ray diffraction (XRD) using a Seifert XRD 3000P for the θ-2θ scans (Cu K_α, $\lambda = 1.5406$ Å). The films were shown to be homogeneous and the structure corresponds to the composition of the target (Ca/Mn = 1) in the limit of accuracy. Sharp and intense diffraction peaks [see Fig. 1(d)] suggest neatly crystallized single-phase films. Using the XRD results, the out-of-plane parameter of the films was calculated to be <3.71 Å, confirming that the films are under tensile strain.

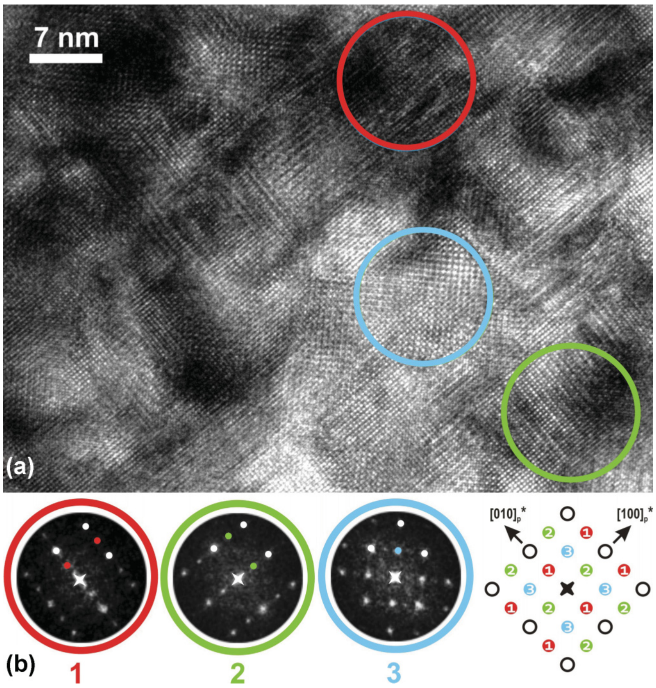

FIG. 2. (Color online) (a) High-resolution TEM image of a $CaMnO_3$ film (thickness 40 nm) revealing regions with a different crystallographic orientation and a lateral extension of a few nanometers. On average, the image possesses a fluctuating contrast suggesting the presence of strain fields due to the nested configuration of the differently oriented regions (Refs. 35 and 36). (b) Fourier transformation obtained from three different areas, corresponding to the three types of orientations of the orthorhombic $CaMnO_3$ unit cell within the film. The schematic drawing summarizes the four different sets of reflections that can be obtained in the Fourier transform of the perovskite subcell (white) and the three orientation variants (color). In total, six orientations of the orthorhombic $CaMnO_3$ unit cell are possible, since *a* and *c* axis may be exchanged within the pseudocubic approximation.

Figure 2 shows a transmission electron microscopy (TEM) image of one of the $CaMnO_3$ films. The TEM image shows that the film is composed of nested regions with a lateral size of $\lesssim$10 nm. Fourier transformation (FT) reveals that there are three different types of regions that are exemplarily highlighted by colored circles. The corresponding states are associated to the three orientations of the orthorhombic unit cell of $CaMnO_3$ with respect to the substrate, that is, with the orthorhombic *b* axis pointing along the *x*, *y*, or *z* direction of the substrate lattice. Applying this assumption, those spots in the FT data that are uniform across the sample are related to a simple cubic perovskite cell. The remaining spots can be explained by applying the distorted $CaMnO_3$ perovskite structure with the same rotations of the MnO_6 octahedra that are present in the bulk. As detailed in Fig. 2(b) the corresponding three sets of spots are then identified as $(h, k/2, 0)$, $(h/2, k, 0)$, and $(h/2, k/2, 0)$. They are associated to [101] (sets 1 and 2) and [010] (set 3) zone axes patterns of the bulk orthorhombic *Pnma* structure with cell parameters $a = \sqrt{2}a_c$, $b = 2a_c$, $c = \sqrt{2}a_c$. Thus, on the one hand, the substrate enforces its cubic lattice parameters onto the $CaMnO_3$ film, but on the other hand, the $CaMnO_3$ retains the bulk orthorhombic atomic distortion for each of its three orientation states.

We recall that, within the pseudocubic approximation, the orthorhombic *a* axis and *c* axis may be interchanged so that we have a total of six possible orientations for the orthorhombic $CaMnO_3$ cell on the $LaAlO_3$ substrate. However, since the resolution of the TEM experiment does not allow us to distinguish between the *a* axis and the *c* axis, only three different orientations are identified in Fig. 2.

Note that the TEM study indicates the presence of a small amount of secondary phase concluded from the observation of supplementary spots along the $\langle 110 \rangle$ direction of the perovskite subcell but not detectable in the XRD data. Such superstructure is compatible with the reduced phases of $CaMnO_3$[37] and is possibly related to the strained state of the film.

IV. SHG ON FERROELECTRIC $CaMnO_3$

Knowing the appropriate framework for the description of our $CaMnO_3$ films, that is, the pseudocubic approximation, we can now derive the possible symmetries of the ferroelectric phase and the resulting polarization selection rules for SHG.

Nonpolar $CaMnO_3$ is centrosymmetric with *mmm* as orthorhombic point symmetry. In the pseudocubic approximation we neglect the difference between the *a* and the *c* axes, which changes the point symmetry to $4/mmm$, with the *b* axis as the fourfold axis. The spontaneous polarization of the strained pseudocubic unit cell may be oriented parallel (case i) or perpendicular to the *b* axis. In the latter case it may be oriented along the principal *a* or *c* axis (case ii) or diagonally, including an angle of 45° with these axes (case iii). Cases (i) or (ii) and case (iii) reduce the point symmetry to $4mm$ and $mm2$, respectively, with "4" and "2" indicating the direction of the spontaneous polarization. Lower symmetries do not have to be considered because they would correspond to other, unphysically arbitrary directions of the spontaneous polarization.

In Table I the SHG contributions for cases (i) to (iii) are given for all the possible orientations of the orthorhombic unit cell within the pseudocubic lattice. Only tensor components χ_{ijk} that can be addressed with light incident perpendicular to the $CaMnO_3$ film ($k \parallel z$) are considered. This excludes all the components with i, j, or $k = z$ since this would involve longitudinally polarized light. Note that the net SHG yield obtained from the $CaMnO_3$ film is a mixture of the SHG contributions for all the orientations of the orthorhombic unit cell that are possible within the pseudocubic lattice.

V. EXPERIMENTAL SETUP

Prior to our SHG experiments, we performed pyroelectric current measurements on the $CaMnO_3$ films. For this purpose, two gold electrodes with a gap of about 1 mm were grown onto the surface of the films. However, as in previous experiments the leakiness of the epitaxial $CaMnO_3$ films in combination with the in-plane geometry spoiled the polarization measurement. This leaves SHG as approach for the detection of a spontaneous polarization.

TABLE I. SHG contributions for all the possible orientations of the orthorhombic b axis and the resulting spontaneous polarization P_{sp} within the pseudocubic lattice. Case (i): P_{sp} of the strained unit cell is oriented parallel to the fourfold b axis. Case (ii): P_{sp} is perpendicular to the b axis and along the principal a or c axis. Case (iii): P_{sp} is perpendicular to the b axis, including an angle of 45° with a and c (these directions are denoted as σ and ρ with $\sigma \perp \rho$). Only tensor components χ_{ijk} that can be addressed with light incident perpendicular to the CaMnO$_3$ film ($k \parallel z$) are considered. This excludes all the components with i, j, or $k = z$ since this would involve longitudinally polarized light.

Pseudocubic direction			SHG contributions
b axis		P_{sp}	accessible with $k \parallel z$
001	(i)	001	0
	(ii)	110	$\rho\rho\rho,\sigma\sigma\rho,\rho\sigma\sigma$
		$1\bar{1}0$	$\sigma\sigma\sigma,\rho\rho\sigma,\sigma\rho\rho$
	(iii)	100	xxx,yyx,xyy
		010	yyy,xxy,yxx
100	(i)	100	xxx,yyx,xyy
	(ii)	011	yyy,xxy,yxx
		$01\bar{1}$	yyy,xxy,yxx
	(iii)	010	yyy,xxy,yxx
		001	0
010	(i)	010	yyy,xxy,yxx
	(ii)	101	xxx,yyx,xyy
		$10\bar{1}$	xxx,yyx,xyy
	(iii)	100	xxx,yyx,xyy
		001	0

In the SHG experiments, frequency-tunable laser pulses of about 130 fs are emitted from an optical parametric amplifier which is operated at 1 kHz by a Ti:sapphire amplifier system. The SHG data are taken in the spectral range $2\hbar\omega =$ 1.8–3.0 eV, which covers the lowest $\text{O}^{2-} \rightarrow \text{Mn}^{4+}$ charge-transfer excitation and the $\text{Mn}^{4+}(t_{2g}) \rightarrow \text{Mn}^{4+}(e_g)$ intraband transfer.[38–40] In order to suppress any surface-induced SHG contributions not coupling to ferroelectric order a near-normal-incidence reflection geometry with a reflection angle incident to the surface normal of approximately 2° is employed. The polarization of the incident laser beam is set by a half-wave plate. Optical filters are chosen to suppress background light in front of the sample and to separate the SHG wave from the fundamental light behind the sample. The polarization of the SHG light is analyzed with a Glan-Taylor prism. For further spectral filtering the signal light is transmitted through a monochromator. It is then detected by a photomultiplier tube and normalized to a reference SHG signal in order to account for spectral variations of the fundamental light and of the efficiency of the SHG setup. In addition, the spectra were normalized by dividing the SHG signal obtained from the sample by the spectrally flat reference SHG response of a silver mirror. Alternatively, for obtaining spatial resolution, the samples were imaged onto a liquid-nitrogen-cooled camera chip using a standard telephoto lens with a resolution of about 25 μm. A liquid-helium-operated cryostat is used to cool the samples to temperatures between 4.5 K and 300 K. Electric fields were applied to the sample via polished steel plates with a diameter of about 1 cm in between which the samples were mounted.

VI. EXPERIMENTAL RESULTS AND DISCUSSION

Prior to the experiments on the CaMnO$_3$ films the SHG response of CaMnO$_3$ and LaAlO$_3$ single crystals was investigated in order to identify any bulk background contributions. As mentioned before, LaAlO$_3$ is a centrosymmetric insulator with a band gap of 5.6 eV[41] and a pseudocubic perovskite subcell that exhibits no ferroic order, so that electric-dipole-type SHG contributions are not expected. In agreement with this, a SHG signal from pure LaAlO$_3$ was not observed in the temperature range from 5 K to 300 K and for photon energies between 1.8 and 3.0 eV. A CaMnO$_3$ single crystal grown by the floating-zone method revealed a spectrally flat, temperature-independent SHG signal that was recorded between 4.5 K and 150 K. It may be related to defects, surface contributions, or SHG contributions beyond the electric-dipole approximation.

Figure 3 shows the normalized spectral, temperature, and polarization dependence of the SHG signal obtained on the epitaxial CaMnO$_3$ films. The pronounced spectral dependence of the SHG signal at 5 K demonstrates that it is not related to the background contribution observed on the CaMnO$_3$ bulk crystals. The spectral dependence is independent of the tensor component. A peak of the SHG intensity is observed at around 2.4 eV, which is probably related to the aforementioned $t_{2g} \rightarrow e_g$ transition of the Mn^{4+} ion.[38–40] For the following experiments a SHG energy of 2.1 eV was chosen because of the high intensity of the fundamental laser beam in combination with a reasonably large SHG yield.

Figure 3(a) shows the temperature dependence of the SHG signal at 2.1 eV. Above 25 K a constant SHG background is obtained that shows an isotropic polarization dependence and is present up to at least 150 K. This is the background signal already observed on the bulk sample and can therefore be regarded as "zero bias" of the SHG measurement. At 25 K a pronounced SHG signal emerges and increases continuously toward 5 K. As Fig. 3(d) reveals, the SHG signal of CaMnO$_3$ has a distinct polarization dependence. The anisotropy measurement shows the SHG yield polarized parallel to the polarization of the incident fundamental light while rotating this polarization by 360°. This leads to four equally long lobes with maximum SHG intensity along the $\langle 110 \rangle$ in-plane-diagonal directions of the pseudocubic lattice. A fit shown as a solid line in Fig. 3(d) reveals that the polarization dependence of the SHG signal is perfectly described by a single SHG tensor component: $\chi_{\rho\rho\rho} = \chi_{\sigma\sigma\sigma}$ (see Table I). This uniquely points to CaMnO$_3$ crystallites with an out-of-plane orientation of the orthorhombic b axis and a spontaneous polarization along the orthorhombic a (respectively c) axis [see Fig. 1(c)]. With two possible in-plane orientations of this polarization the SHG signal from crystallites of either orientation adds up to reveal a fourfold SHG anisotropy in spite of the $mm2$ symmetry of the individual crystallites. This conclusion is in perfect agreement with the predictions made by Bhattacharjee *et al.*[19] and in Sec. VII A. In both cases, density functional theory (DFT) is used to consider an out-of-plane orientation of the

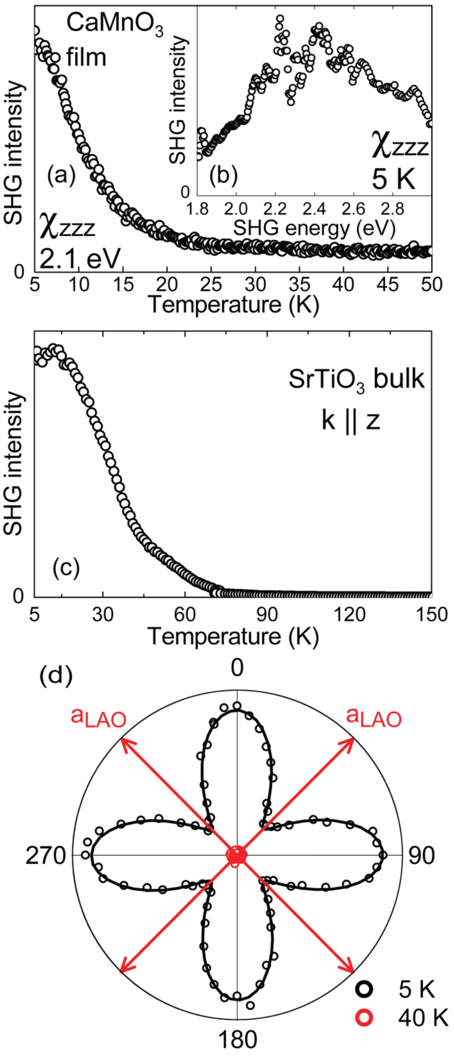

FIG. 3. (Color online) (a) Temperature dependence of the SHG signal at 2.1 eV. At 25 K a pronounced polarized SHG signal emerges and increases continuously toward 5 K. Above 25 K we find a temperature-independent, spectrally featureless SHG background that is present up to at least 150 K. (b) SHG spectrum of χ_{zzz} at 5 K. The resonance at 2.4 eV is probably related to the $t_{2g} \rightarrow e_g$ transition of the Mn^{4+} ion which is also observed in x-ray absorption spectra of bulk CaMnO$_3$ (Ref. 39). (c) Temperature dependence of the SHG signal obtained from incipiently ferroelectric bulk SrTiO$_3$ for comparison. The similarity to the temperature dependence of SHG from CaMnO$_3$ is striking. (d) Polarization dependence of the SHG signal at 5 K and 40 K. The fit entered as black solid line is perfectly described by a single SHG tensor component: $\chi_{\rho\rho\rho} = \chi_{\sigma\sigma\sigma}$ (see Table I).

orthorhombic b axis, and a spontaneous in-plane polarization along the orthorhombic a (respectively c) axis is found.

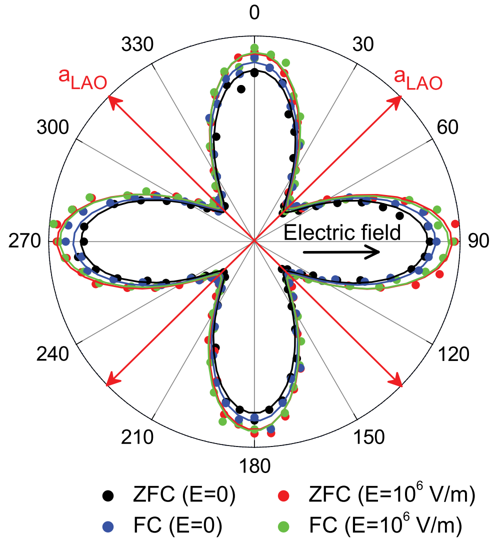

FIG. 4. (Color online) Electric-field dependence of the SHG anisotropy. Samples were zero-field cooled (ZFC, $E = 0$) or field cooled (FC, $E = 10^6$ V/m) from 40 K and measured at 5 K and 2.1 eV with or without the electric field applied. The insensitivity of the SHG signal to the electric field indicates that no polarization switching occurs. Lines are fits to the data according to Fig. 3(d).

Hence, both the SHG data in Fig. 3 and the DFT results point to an electric polarization in the pseudocubic epitaxial CaMnO$_3$ films that is induced by tensile lattice strain of 2.3%. In contrast to the bulk CaMnO$_3$ ground state, the polar mode becomes unstable in the strained film so that a polar displacement can appear. Note that the emergence of the SHG signal below 25 K cannot be due to the magnetic order. First, magnetization-induced SHG can also be observed on the CaMnO$_3$ bulk sample, and its polarization would have to be different from the polarization of the SHG signal in Fig. 3(d). Second, DFT predicted that the antiferromagnetic order and its critical temperature of $T_N = 122$ K are not affected by the substrate strain and the resulting ferroelectric transition.[19] We thus conclude that strained pseudocubic CaMnO$_3$ constitutes a strain-driven multiferroic below 25 K.

In order to investigate the rigidity of the polar state, its response to electric poling fields and thermal cycling was investigated with the results shown in Figs. 4 and 5. Figure 4 shows the effect of a static electric field on the polarization dependence of the SHG signal. The anisotropy of the SHG signal in the absence of an electric field and in a static field of 10^6 V/m during and/or after cooling from 40 K to 5 K is compared. The electric field was applied along, as well as diagonally in between, the directions of the pseudocubic axes. (Only the latter case is depicted here since both cases lead to the same result.) According to Fig. 4, the electric field has no effect on the SHG yield. In addition, cycling the electric field between $\pm 10^6$ V/m showed no sign of polarization reversal or a hysteresis.

Applying an electric field is expected to reverse the polarization of the domains with a polarization component antiparallel to the field and, thus, reduce the number of oppositely polarized domains, ideally toward a single-domain state. Since the SHG signal from oppositely polarized domains interferes destructively,[42] the field poling is therefore expected to *enhance* the SHG yield. Yet, the insensitivity of the SHG signal to the electric field shows that polarization switching does not occur. This may indicate that the polarized regions are so strongly pinned by the substrate strain and the pseudocubic twinning that the applied field is too low for polarization reversal. Yet it is unlikely that even in a field-cooling experiment no tendency at all for the alignment of the spontaneous

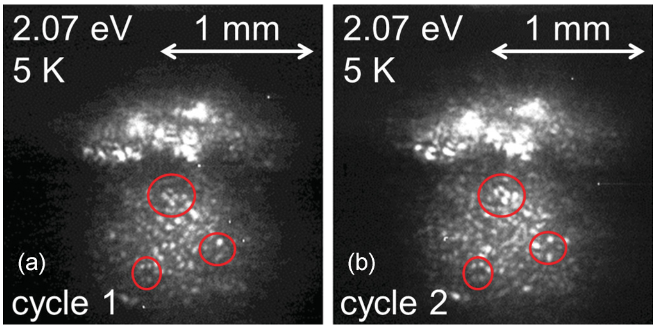

FIG. 5. (Color online) Spatially resolved SHG intensity of a $CaMnO_3$ film at 5 K and 2.07 eV SHG photon energy. A grainy distribution of SHG intensity in the form of resolution-limited speckles is obtained. The relative position and brightness of the speckles does not change after two consecutive cooling cycles through 60 K. The red circles mark exemplary areas.

polarization along the applied field is observed, in particular in view of the large value of the spontaneous polarization (and the related field energy) expected from DFT (Ref. 19 and Sec. VII A).

The spatially resolved SHG intensity of the sample is shown in Fig. 5. The images reveal a grainy distribution of the SHG intensity in the form of resolution-limited speckles. According to Fig. 5(b) the position and relative brightness of the speckles does not change when a consecutive annealing cycle through 60 K is applied. [Note that the arrangement of the speckles in the exemplary red circles is the same in Figs. 5(a) and 5(b).] The result does not change when an electric field is applied during the temperature cycle.

Figure 5 thus reveals that the insensitivity to electric-field cycling is matched by the insensitivity to thermal cycling. Grainy distribution of the SHG intensity is a result of the interference of SHG contributions from areas with a size below the optical resolution limit. Here, these areas can correspond either to the differently oriented crystallographic regions constituting the pseudocubic structure in Fig. 2 or to a distribution of nanometer-sized ferroelectric domains. The similarity of Figs. 5(a) and 5(b) points toward the former. Domains would change in the course of an annealing cycle unless they are strongly pinned. However, as argued before, pinning effects that are pronounced enough to withstand an electric poling field when crossing the Curie temperature in the course of a temperature cycle are unlikely.

We therefore conclude that the polarization picked up by the SHG signal is related to *incipient* ferroelectricity in the strained $CaMnO_3$ films. As we see in the following this conclusion is supported by both experiment and theory. (i) In Fig. 3(c) we show the temperature dependence of the SHG signal from $SrTiO_3$ that we measured for comparison. The retarded emergence of the signal in this incipient ferroelectric is qualitatively very similar to the temperature dependence of the SHG signal from $CaMnO_3$. It is therefore conclusive to expect incipient ferroelectricity to be also present in $CaMnO_3$. (ii) The SHG signal in $SrTiO_3$ displays a distinct spectral and polarization dependence (not shown) just like the SHG signal in $CaMnO_3$. (iii) As confirmed by Fig. 3(c) incipient ferroelectrics can display a pronounced SHG signal although there is no spontaneous polarization breaking the inversion symmetry. (We assume that with the high polarizability characteristic for incipient ferroelectrics the fundamental light wave itself drives the ac polarization that is breaking the inversion symmetry and probed by SHG. This was also proposed for explaining forbidden Raman lines in $KTaO_3$.)[43] In the absence of magnetic or structural transitions in our $CaMnO_3$ films at 25 K, incipient ferroelectricity is thus a compelling reason for the emergence of the SHG signal. (iv) The proximity to the critical strain predicted by DFT[19] is in conformity with a ferroelectric potential that is too shallow to stabilize a spontaneous polarization.

VII. VERIFICATION BY DENSITY FUNCTIONAL THEORY

As mentioned before, the observation of an incipient state with an in-plane polarization along the orthorhombic *a* or *c* axis agrees well with the DFT results reported in Ref. 19. However, in Ref. 19 investigations were limited to $CaMnO_3$ films with an out-of-plane orientation of the orthorhombic *b* axis as shown in Fig. 1(c). Since regions with an in-plane orientation of *b* are present in Fig. 2 we have to expand our DFT analysis now. We do this in two ways: (i) by verifying the results in Ref. 19 using an alternative approach for their derivation and (ii) by adding the scenario of an out-of-plane orientation of *b*. In both cases we retain the pseudocubic approximation of the orthorhombic unit cell.

A. Out-of-plane orientation of the orthorhombic *b* axis

The formerly used pseudopotential approach with the generalized-gradient-approximation (GGA) Wu-Cohen exchange correlation functional [as it is implemented in the ABINIT package] was replaced by the projector-augmented wave (PAW) methodology and the GGA PBEsol[44] exchange correlation functional (as it is implemented in the VASP code).[45,46] Converged results were achieved with a plane-wave cutoff of 500 eV and a *k*-point grid of $4 \times 2 \times 4$. All calculations were performed with collinear magnetism by taking the G-type antiferromagnetic order as the magnetic ground state. Phonon frequencies have been calculated for *Pnma* space group and different values of epitaxial strain using the frozen-phonon method with small atomic displacements of ± 0.03 Å. The cell parameter was imposed to be cubic and fixed to that of the substrate in two directions while it was relaxed in the third direction.

First, we calculated the evolution of the soft transverse-optical (TO) modes versus the epitaxial strain applied along the *a* (respectively *c*) direction [see Fig. 1(c)]. The strain dependence of the square of the frequency Ω of the three soft TO modes (TO_a, TO_b, TO_c) polarized along the three directions of the crystal is shown in Fig. 6. Interestingly, all three modes become softer under tensile epitaxial strain. Within the PBEsol functional the TO_c mode becomes unstable ($\Omega^2 < 0$) at a critical epitaxial strain of 3.7%. This is followed by the TO_a mode, which becomes unstable at 4.0%, whereas the TO_b mode remains stable up to 5.0%, but with a low frequency. This clearly reproduces the fact that $CaMnO_3$ develops a ferroelectric instability under tensile epitaxial strain that is

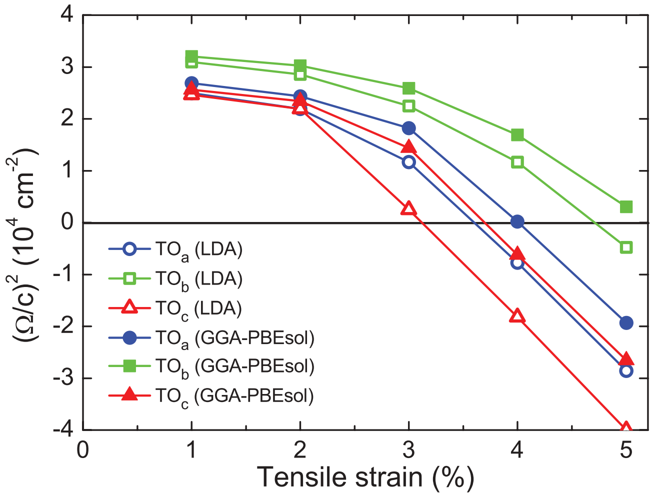

FIG. 6. (Color online) Calculated square of the TO frequency Ω of $CaMnO_3$ versus *a*-*c* epitaxial strain. TO_a, TO_b, and TO_c are the soft TO modes polarized along the orthorhombic *a*, *b*, and *c* axes, respectively. At a critical epitaxial strain of 3.2% (LDA functional) the TO_c mode becomes unstable and initiates a net polarization along the orthorhombic *c* axis (pseudocubic diagonal) reaching 18 $\mu C/cm^2$ at an epitaxial strain of 4%.

resulting in an in-plane polarization. However, we note that the present calculations predict the occurrence of the ferroelectric instability at a critical tensile epitaxial strain of 3.7%. This value is larger than the value of 2.0% derived previously[19] and refers to the *c* instead of the *a* axis. This difference can be related to the different functionals (GGA PBEsol instead of GGA Wu-Cohen) and the different DFT methodology (PAW instead of pseudopotentials) employed here.[47]

In order to scrutinize the influence of the choice of functional, we also performed calculations by the local density approximation (LDA) based on the PBEsol volume: We froze the volume and the cell parameters to the values obtained within the PBEsol functional and performed LDA atomic relaxations and phonon calculations. In Fig. 6 the according values of Ω^2 are shown for the three soft TO modes. We observe the same epitaxial strain sensitivity as reported with the GGA-PBEsol functional. However, now the ferroelectric instabilities develop at a lower epitaxial strain: 3.2% for the TO_c mode, 3.6% for the TO_a mode, and 4.8% for the TO_b mode. The result illustrates the considerable influence the choice of the functional has on the the critical epitaxial strain obtained for the emergence of ferroelectricity. Nevertheless, all calculations show the same trend; that is, a ferroelectric *a*- or *c*-axis instability dominates the response of the $CaMnO_3$ lattice under tensile epitaxial strain applied along the *a* and *c* directions.

The ground state was determined by condensing the unstable modes in the structure once they emerge. We then performed an atomic relaxation for each mode and checked the presence of remaining instabilities. We thus found that up to a tensile strain of 5.0% the ground state is always obtained by the condensation of the TO_c mode alone within the PBEsol and the LDA functionals. Hence, the condensation of the TO_c mode removes all other instabilities. The ferroelectric polarization is then predicted to occur along the in-plane *c* direction. The amplitude of the polarization depends on the value of the epitaxial strain. With the Berry phase method[48] we obtain a spontaneous polarization of 12 $\mu C/cm^2$ with the PBEsol functional and 18 $\mu C/cm^2$ with the LDA functional for an epitaxial strain of 4.0%.

Performing the same analysis as in Table II of Ref. 19 to identify individual atomic contributions to the eigendisplacements of the unstable ferroelectric mode, we also find that the unstable TO_c mode is dominated by Mn and O atomic motions (23% for Mn, 76% for O, and only 1% for Ca at an epitaxial strain of 4% with the PBEsol functional), thus supporting the idea that ferroelectricity in $CaMnO_3$ is mainly driven by the Mn atoms at the B-site, in spite of their partially filled *d* orbitals.[19]

B. In-plane orientation of the orthorhombic *b* axis

Applying the strain along the orthorhombic *b* direction [see Fig. 1(b)] constrains *b* to the *y*-cell parameter of the substrate. The *a* and *c* directions are not parallel to the substrate which constrains their *projection* to the the *x*-cell parameter of the substrate. However, the angle between *a* and *c* can relax since the out-of-plane projections of *a* and *c* are not constrained.[49] For catching this scenario, we performed the calculations on a cell with 40 atoms. Figure 7 shows the evolution of Ω^2 for the three soft TO modes denoted TO_x (mode polarized along the *x* direction of the substrate), $TO_{y(z)}$ (mode polarized along the *y* direction of the substrate with a small component along *z*), and TO_{yz} (mode polarized along the *y* and the *z* directions of the substrate). The TO modes become unstable at critical epitaxial strains of, respectively, 3.6%, 3.8%, and 3.9% within the LDA functional. With the PBEsol functional only the TO_x mode becomes unstable at 4.0%, whereas the $TO_{y(z)}$ mode and the TO_{yz} mode are still stable at this strain. In analogy to the behavior of the TO_c mode

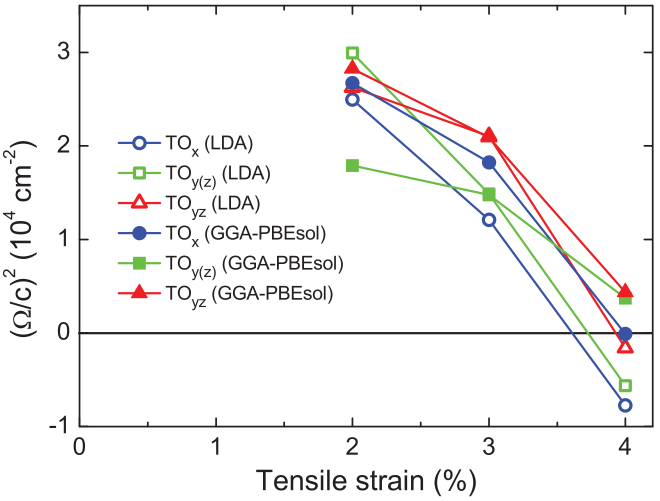

FIG. 7. (Color online) Calculated square of the TO frequency Ω of $CaMnO_3$ versus *b* epitaxial strain. The *x*, *y*, and *z* directions are the directions of the polarization of the modes according to Fig. 1(b). The TO_x mode becomes unstable at a critical epitaxial strain of 3.6% (LDA functional), resulting in a net polarization of 4.6 $\mu C/cm^2$ along the *x* direction of the crystal (pseudocubic axis) at an epitaxial strain of 4%.

with epitaxial strain along a and c, condensing the TO_x mode for strain along b stabilizes the TO_{yz} mode so that the ground state is given by the condensation of the TO_x mode alone. At an epitaxial strain of 4.0% this gives rise to a spontaneous polarization of 4.6 $\mu C/cm^2$ along the in-plane x direction with the LDA functional and a spontaneous polarization of <0.01 $\mu C/cm^2$ with the PBEsol functional.

While the critical epitaxial strain for inducing a ferroelectric instability depends on the exchange-correlation functional and the methodology used, all calculations confirm the SHG results: Independent of the scenario (out-of-plane orientation of b with strain along a and c or in-plane orientation of b with strain along b), a spontaneous polarization along the orthorhombic b direction of the crystal is never stable. Furthermore, a polarization along the x direction with in-plane orientation of b is not observed experimentally. This is consistent with the tendency for the higher values of the epitaxial strain that are required for its occurrence.

Performing the same analysis as for the case where the strain is applied along the a and c directions, the eigendisplacement of the unstable TO_x mode is also found to be strongly dominated by the Mn and O motions: 45% for Mn, 54% for O, and only 1% for Ca at an epitaxial strain of 4% (PBEsol functional).

VIII. CONCLUSION

In summary, epitaxial pseudocubically twinned $CaMnO_3$ films with 2.3% tensile strain were found to be incipiently ferroelectric below 25 K. The polarizability was detected by optical SHG. According to the symmetry analysis of the SHG signal, $CaMnO_3$ crystallites with out-of-plane orientation of the orthorhombic b axis contribute to an emerging polarization directed along the orthorhombic a (respectively c) axis in agreement with a variety of DFT approaches. The antiferromagnetic order as well as the incipient ferroelectric order arise from the Mn^{4+} cation site, which thus creates a remarkable exception to the $3d^0$ rule for perovskite multiferroics. With our experiments we emphasize the potential of strained perovskite oxides as resource for a rich variety of multiferroic compounds. We expect that further research will lead either to constituents with a lower threshold for strain-induced ferroelectricity or to higher values of substrate-induced strain stabilizing the ferroelectric state beyond the incipient behavior found in the $CaMnO_3$ films.

ACKNOWLEDGMENTS

The work at the Universities of Bonn, Liège, and Caen was supported by the STREP MaCoMuFi (MP3-CT-2006-033221) of the European Community. The work was additionally supported in Bonn by the SFB 608 of the DFG and in Liège by EC Project OxIDes (NMP3-SL-2008-228989). Authors in Zurich acknowledge support from ETH Zurich. E.B. thanks the FRS-FNRS Belgium for support. M.F. is grateful for sabbatical support by the IMI Program of the National Science Foundation under Award No. DMR-0843934, managed by the International Center for Materials Research, UC Santa Barbara, USA. Ph.G. thanks the Francqui Foundation for Research Professorship. The authors thank Y. Tomioka (NIAIST, Tsukuba, Japan) and Y. Tokura (University of Tokyo, Japan) for providing the $CaMnO_3$ bulk crystal. They further thank N. A. Spaldin for fruitful discussions and L. Gouleuf for the preparation of the samples used in the TEM experiments.

---

[1] W. Eerenstein, N. D. Mathur, and J. F. Scott, Nature (London) **442**, 759 (2006).

[2] S. W. Cheong and M. Mostovoy, Nat. Mater. **6**, 13 (2007).

[3] N. Hill, J. Phys. Chem. B **104**, 6694 (2000).

[4] A. Filippetti and N. A. Hill, Phys. Rev. B **65**, 195120 (2002).

[5] D. Khomskii, Physics **2**, 20 (2009).

[6] R. Newnham, J. Kramer, W. Schulze, and L. Cross, J. Appl. Phys. **49**, 12 (1978).

[7] T. Kimura, T. Goto, H. Shintani, K. Ishizaka, T. Arima, and Y. Tokura, Nature (London) **406**, 55 (2003).

[8] N. Hur, S. Park, P. A. Sharma, J. S. Ahn, S. Guha, and S. W. Cheong, Nature (London) **429**, 392 (2004).

[9] C. Jia, S. Onoda, N. Nagaosa, and J. H. Han, Phys. Rev. B **76**, 144424 (2007).

[10] D. G. Schlom, L. Q. Chen, C. B. Eom, K. M. Rabe, S. K. Streiffer, and J.-M. Triscone, Annu. Rev. Mater. **37**, 589 (2007).

[11] K. J. Choi, M. Biegalski, Y. L. Li, A. Sharan, J. Schubert, R. Uecker, P. Reiche, Y. B. Chen, X. Q. Pan, V. Gopalan L. Q. Chen, D. G. Schlom, and C. B. Eom, Science **306**, 1005 (2004).

[12] R. S. Beach, J. A. Borchers, A. Matheny, R. W. Erwin, M. B. Salamon, B. Everitt, K. Pettit, J. J. Rhyne, and C. P. Flynn, Phys. Rev. Lett. **70**, 3502 (1993).

[13] D. Fuchs, E. Arac, C. Pinta, S. Schuppler, R. Schneider, and H. von Loehneysen, Phys. Rev. B **77**, 014434 (2008).

[14] J. Haeni, P. Irvin, W. Chang, R. Uecker, P. Reiche, Y. Li, S. Choudhury, W. Tian, M. Hawley, B. Craigo *et al.*, Nature (London) **430**, 758 (2004).

[15] C. Thiele, K. Dorr, O. Bilani, J. Rodel, and L. Schultz, Phys. Rev. B **75**, 054408 (2007).

[16] J. Lee, L. Fang, E. Vlahos, X. Ke, Y. Jung, L. Kourkoutis, J.-W. Kim, P. Ryan, T. Heeg, M. Roeckerath *et al.*, Nature (London) **466**, 954 (2010).

[17] C. J. Fennie and K. M. Rabe, Phys. Rev. Lett. **97**, 267602 (2006).

[18] E. Bousquet, N. A. Spaldin, and P. Ghosez, Phys. Rev. Lett. **104**, 037601 (2010).

[19] S. Bhattacharjee, E. Bousquet, and P. Ghosez, Phys. Rev. Lett. **102**, 117602 (2009).

[20] H. Sakai, J. Fujioka, T. Fukuda, D. Okuyama, D. Hashizume, F. Kagawa, H. Nakao, Y. Murakami, T. Arima, A. Baron *et al.*, Phys. Rev. Lett. **107**, 137601 (2011).

[21] T. Sakudo and H. Unoki, Phys. Rev. Lett. **26**, 851 (1971).

[22] H. Uwe, H. Unoki, Y. Fujii, and T. Sakudo, Solid State Commun. **13**, 737 (1973).

[23] H. Uwe and T. Sakudo, Phys. Rev. B **13**, 271 (1976).

[24] A. S. Chaves, F. C. S. Barreto, and L. A. A. Ribeiro, Phys. Rev. Lett. **37**, 618 (1976).

[25] V. V. Lemanov, A. V. Sotnikov, E. P. Smirnova, and M. Weihnacht, Appl. Phys. Lett. **81**, 886 (2002).

[26] K. A. Müller and H. Burkard, Phys. Rev. B **19**, 3593 (1979).

[27] W. Zhong and D. Vanderbilt, Phys. Rev. B **53**, 5047 (1996).

[28] V. V. Lemanov, A. V. Sotnikov, E. P. Smirnova, M. Weihnacht, and R. Kunze, Solid State Commun. **110**, 611 (1999).

[29] R. Viana, P. Lunkenheimer, J. Hemberger, R. Böhmer, and A. Loidl, Phys. Rev. B **50**, 601 (1994).

[30] M. Fiebig, V. Pavlov, and R. Pisarev, J. Opt. Soc. Am. B **22**, 96 (2005).

[31] T. Kordel, C. Wehrenfennig, D. Meier, T. Lottermoser, M. Fiebig, I. Gelard, C. Dubourdieu, J.-W. Kim, L. Schultz, and K. Dorr, Phys. Rev. B **80**, 045409 (2009).

[32] Y. Shen, *The Principles of Nonlinear Optics* (Wiley, New York, 2002).

[33] Y. Uesu, S. Kurimura, and Y. Yamamoto, Appl. Phys. Lett. **66**, 2165 (1995).

[34] K. Poeppelmeier, M. Leonowicz, J. Scanlon, and J. Longo, J. Solid State Chem. **45**, 71 (1982).

[35] E.-L. Rautama, P. Boullay, A. Kundu, V. Caignaert, V. Pralong, M. Karppinen, and B. Raveau, Chem. Mater. **20**, 2742 (2008).

[36] J. Scola, P. Boullay, W. Noun, E. Popova, Y. Dumont, A. Fouchet, and N. Keller, J. Appl. Phys. **110**, 043928 (2011).

[37] A. Reller, J. Thomas, D. Jefferson, and M. Uppal, Proc. R. Soc. London A **394**, 223 (1984).

[38] S. Satpathy, Z. S. Popović, and F. R. Vukajlović, Phys. Rev. Lett. **76**, 960 (1996).

[39] G. Zampieri, M. Abbatec, F. Pradoa, A. Caneiroa, and E. Morikawad, Physica B: Condens. Matter **320**, 51 (2002).

[40] N. N. Loshkareva, L. V. Nomerovannaya, E. V. Mostovshchikova, A. A. Makhnev, Y. P. Sukhorukov, N. I. Solin, T. I. Arbuzova, S. V. Naumov, N. V. Kostromitina, A. M. Balbashov *et al.*, Phys. Rev. B **70**, 224406 (2004).

[41] S.-G. Lim, S. Kriventsov, T. Jackson, J. Haeni, D. Schlom, A. Balbashov, R. Uecker, P. Reiche, J. Freeout, and G. Lucovsky, J. Appl. Phys. **91**, 4500 (2002).

[42] M. Fiebig, D. Fröhlich, T. Lottermoser, and M. Maat, Phys. Rev. B **66**, 144102 (2002).

[43] A. R. Akbarzadeh, L. Bellaiche, K. Leung, J. Íñiguez, and D. Vanderbilt, Phys. Rev. B **70**, 054103 (2004).

[44] J. P. Perdew, A. Ruzsinszky, G. I. Csonka, O. A. Vydrov, G. E. Scuseria, L. A. Constantin, X. Zhou, and K. Burke, Phys. Rev. Lett. **100**, 136406 (2008).

[45] G. Kresse and J. Furthmüller, Phys. Rev. B **54**, 11169 (1996).

[46] G. Kresse and D. Joubert, Phys. Rev. B **59**, 1758 (1999).

[47] J. Hong, A. Stroppa, J. Íñiguez, S. Picozzi, and D. Vanderbilt, Phys. Rev. B **85**, 054417 (2012).

[48] R. D. King-Smith and D. Vanderbilt, Phys. Rev. B **47**, 1651 (1993).

[49] C.-J. Eklund, C. J. Fennie, and K. M. Rabe, Phys. Rev. B **79**, 220101 (2009).